

1 **Nutrient availability in the North Pacific region not primarily driven by climate through the**  
2 **Quaternary**

3

4 **Andrea M. Snelling<sup>1\*</sup>, George E. A. Swann<sup>1</sup>, Vanessa Pashley<sup>2</sup>, Jack H. Lacey<sup>2</sup>, Matthew S.A.**  
5 **Horstwood<sup>2</sup>, Melanie J. Leng<sup>2,3</sup>**

6 <sup>1</sup> School of Geography, University of Nottingham, Nottingham, NG7 2RD, UK

7 <sup>2</sup> National Environmental Isotope Facility, British Geological Survey, Keyworth, Nottingham, NG12 5GG, UK

8 <sup>3</sup> School of Biosciences, University of Nottingham, Sutton Bonington Campus, Loughborough, NE12 5RD, UK

9 \* Corresponding author: andrea.snelling2@nottingham.ac.uk

10

11 **Keywords**

12 North Pacific; Silicon isotope; biogeochemical cycling; nutrient utilisation; ocean stratification;  
13 Mid-Pleistocene Transition

14

15 **Abstract**

16 The subarctic North Pacific Ocean is a relatively understudied region in terms of palaeoclimate,  
17 limiting our understanding of how the region has both driven and responded to  
18 palaeoenvironmental events. Today, the subarctic North Pacific Ocean is marked by a year round  
19 stratified water column with a halocline at c. 300 m water depth. Previous studies at ODP Site 882  
20 in the Northwest Pacific have suggested the stratified water column system developed at the  
21 onset of major Northern Hemisphere Glaciation (2.73 Ma). In addition to limiting the upwelling of  
22 carbon-rich deep waters and associated ventilation of CO<sub>2</sub> to the atmosphere, the shift to a

23 stratified state fundamentally altered oceanographic conditions and biogeochemical cycling across  
24 the region. Key questions remain over whether the region was permanently stratified for all of the  
25 Quaternary, or whether the changes in stratification/biogeochemical cycling altered over major  
26 climatic transitions such as the Mid-Pleistocene Transition (MPT), a process that would alter  
27 regional ocean-atmospheric carbon exchanges. We present new silicon and oxygen isotope data  
28 from diatoms ( $\delta^{30}\text{Si}_{\text{diatom}}$  and  $\delta^{18}\text{O}_{\text{diatom}}$ ), alongside previously published data in order to test the  
29 mechanisms of biogeochemical cycling in the subarctic North Pacific Ocean between 2.85 Ma and  
30 0.06 Ma, including influences from the wider region such as Glacial North Pacific Intermediate  
31 Water (GNPIW) originating in the Bering Sea. This has enabled us to reconstruct temporal changes  
32 in photic zone nutrient utilisation and silicic acid supply in the northwest subarctic Pacific Ocean  
33 through the progressive intensification of glacial-interglacial cycles through the Quaternary and  
34 over the MPT. We show that prior to the MPT climate does not appear to be a primary controller  
35 of nutrient availability in the North Pacific region, but that following the MPT, it has a greater  
36 influence, shown by the interrelationship with the upwelling index from the Bering Sea.

37

## 38 **1. Introduction**

39 The history of the subarctic north-west Pacific Ocean, has been relatively understudied compared  
40 to other marine locations due to the poor preservation of calcareous fossils (Haug et al., 1999,  
41 Swann, 2010). Over the past two decades, evidence has emerged as to the region's potential role  
42 as a driver of global climatic change through oceanic-atmospheric exchanges in  $\text{CO}_2$  (Jaccard et al.,  
43 2005, Galbraith et al., 2008, Gebhardt et al., 2008, Swann, 2010, Gong et al., 2019). The area today  
44 (Figure 1) is marked by a year round stratified water column at c. 300 m water depth as a result of  
45 a strong vertical salinity gradient (halocline). Recent studies using Argo profiling float data suggest

46 that the modern halocline has distinct zonal patterns in terms of depth and intensity, with  
47 intensification of the halocline occurring in late winter (Katsura et al., 2020). In the past, the  
48 absence of a halocline (e.g. during the Pliocene) would have allowed significant upwelling of  
49 nutrient and CO<sub>2</sub> rich deep water to the surface, helping to maintain the warm Pliocene climate  
50 state (Haug et al., 1999).

51 Although the development of the halocline at the onset of major Northern Hemisphere Glaciation  
52 (NHG) (2.73 Ma) inhibited the upwelling of this North Pacific Deep Water (NPDW) and helped  
53 lower atmospheric *p*CO<sub>2</sub> (Haug et al., 1999; Sigman et al., 2004; Haug et al 2005), the subsequent  
54 history of subarctic Pacific Ocean stratification is poorly constrained (Swann, 2010). There is  
55 evidence of periodic breakdowns in the halocline during the late Quaternary (Sarnthein et al.,  
56 2004; Jaccard et al., 2005, 2009, 2010; Galbraith et al., 2007, 2008; Gebhardt et al., 2008; Brunelle  
57 et al., 2010; Swann and Snelling, 2015), including the last deglaciation (Gray et al., 2018, Rae et al.,  
58 2020), but there are few data relating to the intervening period. Any changes in stratification will  
59 have affected the biological pump, which is responsible for the removal of nutrients and CO<sub>2</sub> from  
60 the surface waters into the ocean interior and plays a vital role in regulating the climate through  
61 ocean/atmosphere interactions (Sigman and Hain, 2012).

62 In addition to the halocline, recent work has also pointed to the role of Glacial North Pacific  
63 Intermediate Water (GNPIW) in controlling North Pacific Deep Water (NPDW) upwelling and  
64 consequently releases of CO<sub>2</sub> to the atmosphere during glacials over the past 1.2 Ma (Knudsen and  
65 Ravello 2015a, Worne et al 2019, 2020). GNPIW is a dense water mass formed as a result of brine  
66 rejection during winter sea ice production in the Bering Sea (Warner and Roden, 1995, Shcherbina  
67 et al., 2003), taking atmospherically equilibrated oxygen to the ocean interior (Knudson and  
68 Ravello, 2015a). It is thought to propagate southwards into the open ocean through the  
69 Kamchatka Strait (Horikawa et al., 2010, Jang et al., 2017) and further limits NPDW upwelling and

70 primary productivity in surface waters (Worne et al., 2019, 2020) (Figure 2). The name GNPIW  
71 distinguishes this water from NPIW which originates in the Sea of Okhotsk and then spreads  
72 eastwards into the North Pacific towards the California current region (Max et al., 2014).  
73  
74 Currently, the long-term evolution of the subarctic Pacific halocline, the expansion of  
75 GNPIW/NPIW into the subarctic Pacific and their combined impact on nutrient dynamics through  
76 the early Quaternary is poorly understood. Constraining these changes is key, not only to  
77 understand the timing of NPDW upwelling and release of CO<sub>2</sub> to the atmosphere, but also the role  
78 of nutrient availability and the biological pump in mediating such activity and exporting carbon  
79 from the photic zone (productivity zone above the halocline) into the deep ocean/sediment record  
80 (Volk and Hoffert, 1985; Sigman et al., 2010). In particular, the role and response of the subarctic  
81 Pacific Ocean over the Mid-Pleistocene Transition (MPT) (1.25-0.7 Ma) remains unclear, although  
82 recent studies in the Bering Sea have begun to address this (Worne et al., 2019, 2020). The MPT  
83 marks a significant change in Earth's climate history as the glacial-interglacial cycles migrate from  
84 small-amplitude 41 ky cycles to a dominance of larger amplitude, asymmetric 'saw-tooth' 100 ky  
85 glacial-interglacial cycles. Climate records suggest that there were no significant shifts in solar  
86 radiation as a result of orbital variations to cause this change in glacial periodicity, but instead the  
87 climate system developed an enhanced sensitivity to orbital forcing at this time (Ravelo et al.,  
88 2004, Mc Clymont et al., 2013). The internal mechanisms and teleconnections behind the  
89 transition from 41 ky to 100 ky glacial-interglacial cycles are still much debated (McClymont et al.,  
90 2013) and include a threshold response to atmospheric CO<sub>2</sub> concentrations (Raymo, 1997), a  
91 change in global ice sheet dynamics (Clark and Pollard, 1998; Raymo et al., 2006; Crowley and  
92 Hyde, 2008), and other feedbacks related to deep-water cooling, thermocline depth, sea-ice  
93 distributions and atmospheric circulation (Tziperman and Gildor, 2003; McClymont and Rosell-

94 Melé, 2005; Lee and Poulsen, 2006; McClymont et al., 2013, Kender et al. ,2018, Worne et al.,  
95 2020).

96

97 Here we present diatom oxygen and silicon isotope data ( $\delta^{18}\text{O}_{\text{diatom}}$  and  $\delta^{30}\text{Si}_{\text{diatom}}$ ) from ODP Site  
98 882, alongside previously published data sets from the Late Quaternary (Swann and Snelling 2015)  
99 and Late Pliocene/Early Quaternary (Swann 2010, Bailey et al., 2011). Changes in  $\delta^{18}\text{O}_{\text{diatom}}$  can be  
100 used to reflect changes in oceanographic conditions (ocean mass, fresh water, temperature)  
101 including changes in stratification state, whilst  $\delta^{30}\text{Si}_{\text{diatom}}$  records changes in productivity linked to  
102 photic zone silicic acid utilisation, which is dependent on the supply and biological demand for  
103 silicic acid (Reynolds et al., 2006). These data are used to investigate the relationship between  
104 changes in the biological pump, GNPIW/NPIW propagation and halocline stratification in the  
105 north-west subarctic Pacific through the Quaternary and over the MPT.

106

## 107 **2. Material and methods**

108 ODP Site 882 is situated on the western section of the Detroit Seamounts at a water depth of  
109 3,244m (50°22' N, 167°36' E) (Figure 1). The age model for this core comes from astronomically  
110 calibrated high-resolution gamma-ray attenuation porosity evaluator (GRAPE) density and  
111 magnetic susceptibility measurements (Tiedemann and Haug, 1995). The period from 0-0.8 Ma is  
112 then refined using higher resolution benthic foraminifera  $\delta^{18}\text{O}$  that corroborate the tuned  
113 stratigraphy and by visually matching common inflection points between ODP Site 882 biogenic  
114 barium data and EPICA Dome C  $\delta D$  (Jaccard et al., 2005, 2009, 2010).

115

116 Sixty-six samples from ODP Site 882 between the ages of 0.48 and 2.48 Ma were prepared for  
117 diatom isotope analysis. Samples were chosen to encompass both glacial and interglacial periods  
118 through the Quaternary and were cleaned using a combination of heavy liquid separation,

119 hydrogen peroxide and hydrochloric acid (Swann et al., 2013). Samples were further sieved at 53  
120  $\mu\text{m}$  and 20  $\mu\text{m}$  to remove sponge spicules and radiolaria, which may have different isotopic  
121 fractionation factors to diatoms (e.g. de la Rocha, 2003, Snelling et al., 2014, Cassarino et al.,  
122 2018), and checked using a Zeiss Axiovert 40 C inverted microscope, scanning electron microscope,  
123 and X-ray fluorescence to confirm sample purity and the absence of non-diatom contaminants.  
124 Samples with an XRF Al/Si ratio of  $\leq 0.03\%$  were retained for isotope analysis (Figure 3). Previous  
125 studies have considered and discounted the impact of species effects on both  $\delta^{18}\text{O}_{\text{diatom}}$  and  
126  $\delta^{30}\text{Si}_{\text{diatom}}$  (Swann et al., 2008, Maier et al 2013, Grasse et al., 2021 ) and indicate that detailed  
127 assemblage data is useful in interpreting isotope data. Here, all samples contained a variety of  
128 similar diatom species, therefore we consider any species effects to be negligible.

129

130 Samples were digested and prepared for  $\delta^{30}\text{Si}_{\text{diatom}}$  analysis following methods outlined in Panizzo et  
131 al. (2016) To overcome any analytical bias, sample and reference materials are acidified using HCl  
132 (to a concentration of 0.05M, using twice quartz-distilled acid) and sulphuric acid (to a  
133 concentration of 0.003M, using Romil Ultra Purity Acid and all samples are doped with  $\sim 300\text{ppb}$   
134 magnesium (Mg, Alfa Aesar SpectraPure) to correct for the effects of instrument induced mass  
135 bias, (Hughes, 2011). Analyses were carried out on a ThermoScientific Neptune Plus MC-ICP-MS  
136 (multi collector inductively coupled plasma mass spectrometer) at the National Environmental  
137 Isotope Facility (NEIF) at the British Geological Survey (UK), operated in wet plasma mode using  
138 the method/settings outlined in Cockerton et al. (2013) and Panizzo et al. (2016). In brief, the data  
139 are acquired using a dynamic, two sequence, acquisition. Faraday amplifier gains are measured at  
140 the beginning of each analytical session and data are collected as 1 block of 20 ratios measured at  
141 16.8 second integrations for Si and 8.4 seconds for Mg. The blank contribution is measured on the  
142 sample make-up acid (0.05M HCl, 0.003M  $\text{H}_2\text{SO}_4$ ) using a shortened version of the acquisition

143 procedure. An on-line background correction is made, with the values obtained for the blank acid  
144 subtracted from the succeeding sample.

145  
146 NBS-28 is employed as the primary reference material and Diatomite as the validation material;  
147 both of which are analysed repeatedly during each analytical session.

148  
149  $\delta^{18}\text{O}_{\text{diatom}}$  was obtained using a step-wise fluorination method also at the NEIF with measurements  
150 made on a Thermo Finnigan MAT 253 and values converted to the VSMOW scale using the NEIF  
151 within-run laboratory diatom standard  $\text{BFC}_{\text{mod}}$  which has been calibrated against NBS28 (Leng and  
152 Sloane, 2008). Analytical error is 0.3‰ ( $1\sigma$ ) for oxygen analysis (Leng and Sloane, 2008) and  
153 0.15‰ ( $2\sigma$ ) for silicon.

154

## 155 **2.1 Silicon isotope fractionation**

156 Silicon isotope fractionation by organisms can occur within a closed or open system. In an ‘open’  
157 system, under steady state conditions, there is a continuous supply of nutrients to the photic zone,  
158 whereas in a closed system the supply of nutrients is finite and fractionation occurs along a  
159 Rayleigh distillation curve. Historically, it has been accepted that following the onset of major NHG  
160 at 2.73 Ma, the formation of the halocline was a permanent feature of the subarctic North Pacific  
161 Ocean and its presence would suggest that the area is representative of a closed system given that  
162 the halocline restricts mixing between deep and surface water (productivity zone), thus creating  
163 an environment with a finite supply of nutrients. In this case changes in  $\delta^{30}\text{Si}_{\text{diatom}}$  can be  
164 represented by:

165

$$166 \quad \delta^{30}\text{Si}_{\text{diatom}} = \delta^{30}\text{Si}(\text{OH})_4 \text{ initial} - \varepsilon \cdot (f \ln f / (1 - f)) \quad (\text{Eq. 1})$$

167

168 where  $\delta^{30}\text{Si}(\text{OH})_4$  initial is initial silicic acid in the surface water (derived from upwelled NPDW).  
169 Reynolds et al (2009) use a mean value of 1.63‰ for surface water upwelled from NPDW in their  
170 models because the Si isotope value is not fixed or homogenized at the surface and is the value  
171 that we use here for  $\delta^{30}\text{Si}(\text{OH})_4$  initial. We assume that this value has not changed over time,  $\epsilon$  is  
172 the fractionation factor between the dissolved and particulate phase [−1.1‰: De la Rocha et al  
173 (1997)] and  $f$  is the fraction of silicic acid remaining in the surface ocean. Silicic acid utilisation can  
174 then be calculated as  $(1 - f)$ .

175

176 With  $\delta^{30}\text{Si}_{\text{diatom}}$  a function of both nutrient utilisation and supply to the photic zone, changes in the  
177 supply of silicic acid can be calculated relative to the oldest sample referred to in this study (2.85  
178 Ma) by normalising rates of nutrient utilisation against opal/biogenic rates of siliceous productivity  
179 (Horn et al., 2011):

180

$$181 \quad \text{Si}(\text{OH})_4(\text{supply}) = \frac{\text{Opal}_{\text{sample}}/\text{Opal}_{2.85 \text{ Ma}}}{\text{Si}(\text{OH})_4(\text{utilisation sample})/\text{Si}(\text{OH})_4(\text{utilisation } 2.85 \text{ Ma})} * \frac{\text{Si}(\text{OH})_4^{\text{Present Deep}}}{\text{Si}(\text{OH})_4^{\text{Sample}}} \quad (\text{Eq. 2})$$

182

183 The oldest sample was chosen to normalise the data as this is prior to the formation of the  
184 halocline and represents an open ocean system, when nutrient supply and productivity would  
185 have been high. Using the above equations, silicic acid utilisation and supply was calculated for the  
186 new samples measured in this study as well as for the previously measured samples from the Late  
187 Quaternary (Swann and Snelling 2015) and from the Late Pliocene/Early Quaternary (Swann 2010,  
188 Bailey et al., 2011). For  $\text{Si}(\text{OH})_4^{\text{Present Deep}}$  we use the modern subarctic Pacific value at 1,500 m of  
189 174.2  $\mu\text{M}$  (Reynolds et al., 2006) and we assume that past  $\text{Si}(\text{OH})_4$  concentrations were the same  
190 as today. Opal (%wt) data is an amalgamation of existing data from Tiedermann and Haug (1995),



191 Haug et al., (1995) and Jaccard et al., (2005, 2009, 2010), in addition to new data from this study  
192 measured on freeze dried sediment samples, following wet alkaline digestion and UV/VIS  
193 spectrophotometry. Where required, opal values for individual samples were obtained by linear  
194 interpolation from the combined opal datasets.

195

## 196 **2.2 Oxygen isotope correction**

197 To ensure that changes in  $\delta^{18}\text{O}_{\text{diatom}}$  reflect local surface oceanographic conditions, all values from  
198 this study and existing  $\delta^{18}\text{O}_{\text{diatom}}$  values (Swann and Snelling 2015, Swann, 2010, Bailey et al., 2011)  
199 were corrected for whole ocean changes in  $\delta^{18}\text{O}$  using the LR04 benthic foraminifera  $\delta^{18}\text{O}$  dataset  
200 (Lisiecki and Raymo, 2005). In addition, changes in sea surface temperature (SST) were corrected  
201 relative to the temperature of the oldest sample at 2.85 Ma, using  $\text{U}^{k}_{37}$  SST reconstructions from  
202 ODP Site 882 (Haug et al., 2005) with a  $\delta^{18}\text{O}_{\text{diatom}}$  temperature coefficient of  $-0.2\text{‰}/^{\circ}\text{C}$  (Brandriss  
203 et al., 1998; Moschen et al., 2005).

204

## 205 **3. Results**

### 206 **3.1 $\delta^{30}\text{Si}_{\text{diatom}}$**

207 Over the presented interval (0.06-2.85 Ma), there are significant changes in  $\delta^{30}\text{Si}_{\text{diatom}}$  with values  
208 fluctuating between 0.5 ‰ and 1.7 ‰ (Figure 4). Fluctuations occur throughout the record with  
209 the biggest changes occurring around 0.06-0.15 Ma, 0.54-0.62 Ma, 0.92-1.0 Ma, 1.19-1.26 Ma,  
210 1.54-1.64 Ma and 2.56-2.75 Ma. The lowest  $\% \text{Si}(\text{OH})_4$  utilisation values occur following NHG (2.55-  
211 2.60 Ma), with subsequent fluctuations predominantly in interglacial periods. There are fewer  
212 isotope data between 1.63 Ma and 2.48 Ma due to the low opal concentrations and poor diatom  
213 preservation over this period. The intervals of high fluctuation occur when there is variable opal

214 concentration (Figure 4), but there is no firm relationship between  $\delta^{30}\text{Si}_{\text{diatom}}$  and opal ( $r^2 = 0.05$ ).  
215 Between 0.06 Ma – 0.2 Ma  $\% \text{Si(OH)}_4$  utilisation drops to values similar to the start of the Quaternary.  
216  
217 The supply of silicon to the photic zone follows changes in opal concentrations, with peaks in  
218 supply at 0.12 Ma, 0.70-0.71 Ma, 0.84-1.05 Ma, 1.23-1.26 Ma, 1.45-1.59 Ma and 2.6 Ma.  
219 Comparison of the  $\% \text{Si(OH)}_4$  utilisation and  $\text{Si(OH)}_4$  supply show little relationship with high and low  
220 utilisation occurring under both high and low nutrient supply (Figure 5b) ( $R^2 = 0.001$ ). Silicon  
221 supply and utilisation were also calculated under an open system scenario, to constrain silicon  
222 dynamics in an unstratified water column state, and we found similar trends in the data (see  
223 supplementary data). This means that if the ocean state did change to an open system during the  
224 Quaternary, the closed system trends reported in this study remain valid.

225

### 226 **3.2 $\delta^{18}\text{O}_{\text{diatom}}$**

227 The  $\delta^{18}\text{O}_{\text{diatom}}$  record has distinct peaks over the analysed interval, with values fluctuating  
228 between 46.2‰ and 34.5‰ (Figure 4). The biggest changes occur at 0.07-0.11 Ma, 0.92-0.96 Ma,  
229 1.05-1.26 Ma, 2.28-2.40 Ma, 2.4-2.28 Ma and 2.63-2.69 Ma, with high and low values apparent in  
230 both glacial and interglacial periods. The SST normalised  $\delta^{18}\text{O}_{\text{diatom}}$  values show that despite the  
231 significant change in temperature over the analysed interval (between 1.8 and 18.2°C), this can  
232 only account for up to 3.3‰ of the change in  $\delta^{18}\text{O}_{\text{diatom}}$ , based on a  $\delta^{18}\text{O}_{\text{diatom}}$  temperature  
233 coefficient of  $-0.2\text{‰}/^\circ\text{C}$  (Brandriss et al., 1998; Moschen et al., 2005). Therefore, the range of  
234  $\delta^{18}\text{O}_{\text{diatom}}$  (up to 11.7‰) is evidence of significant changes in photic zone seawater  $\delta^{18}\text{O}$  at ODP  
235 Site 882.

236

## 237 **4. Discussion**

238 Marine diatoms are responsible for up to 70% of primary productivity (Nelson et al., 1995) and  
239 play an important role in organic carbon export production (Smetacek 1999). Consequently,  
240 considering the supply and utilisation of nutrients by diatoms provides an indication of the  
241 strength of the past biological pump and ocean-atmospheric exchanges of CO<sub>2</sub>. The modern North  
242 Pacific Ocean is a high-nitrate, low-chlorophyll region (HNLC) and as such diatom/opal  
243 productivity can be limited by iron (Fe) and light (Tsuda et al., 2003, Lam et al., 2013; Wang et al.,  
244 2019). The delivery of Fe to the subarctic Pacific may have changed on glacial-interglacial  
245 timescales (Kohfeld and Chase, 2011). Productivity is also linked to regional ocean stratification  
246 (halocline) and the presence/absence of GNPIW/NPIW in this region, which impedes the upwelling  
247 of nutrient rich NPDW. Worne et al. (2019, 2020) created an upwelling index for the Bering Sea,  
248 finding that decreased upwelling and nutrient availability during glacial periods was a result of  
249 increased sea ice and GNPIW formation. Further comparisons have shown a correlation between  
250 changes in subarctic Pacific opal concentrations at ODP Site 882 and Bering Sea upwelling (Worne  
251 et al., 2019, 2020) with broadly similar interglacial peaks 0.48-0.8 Ma, but less association for the  
252 remaining record. This suggests that the influence of Bering Sea GNPIW in the wider subarctic  
253 North Pacific is variable and that prior to 1 Ma, climate does not play a primary role in either  
254 nutrient availability or GNPIW formation in the North Pacific Ocean, given the disassociation  
255 between the climate cycles and the upwelling peaks at this time. The role of the halocline,  
256 however, may have had a greater influence on nutrient availability.

257

258 Diatom/opal concentrations in the ocean sedimentary record are also influenced by export  
259 production and preservation. Following the collapse in biogenic opal concentrations at 2.73 Ma in  
260 the North Pacific (Haug et al., 1999) and opal deposition to other areas (Cortese et al., 2004),  
261 Quaternary opal concentrations generally remained low, but show significant peaks (1.53 Ma, 1.28

262 Ma, 1.04 Ma, 0.91 Ma, 0.71 Ma) (%BSi Figure 4) indicating enhanced productivity and/or  
263 favourable opal preservation in the North Pacific (Haug et al., 1995; Jaccard et al., 2010). The  
264 degree to which GNPIW/NPIW and the halocline played a role in controlling upwelling and export  
265 production at ODP Site 882 can be investigated using the silicic acid supply and utilisation data  
266 calculated from  $\delta^{30}\text{Si}_{\text{diatom}}$  and their inter-relationships. These data can constrain the activity and  
267 efficiency of the silicon and biological pump to provide insight to the contribution of the region to  
268 influencing/regulating global climate change, through ocean/atmosphere exchanges of  $\text{CO}_2$ .

269

#### 270 **4.1 Early Quaternary records**

271 Following the NHG at 2.73 Ma opal productivity in the photic zone dropped from an average of 66  
272 %wt (2.74-3 Ma) to 19 %wt (0-2.73 Ma) which has been attributed to the formation of the  
273 halocline, limiting upwelling of nutrients from deep water into the photic zone (Haug et al., 2005).  
274 From 2.73-2.55 Ma, previously published records (Bailey et al., 2011) suggested that an increase in  
275 iron deposition raised the biological demand for nitrate relative to silicic acid (Figure 5A),  
276 accompanied by a change in the ratio of nutrients supplied to the photic zone, which led to under-  
277 utilisation of silicic acid, reflected in the  $\% \text{Si}(\text{OH})_4 \text{ utilisation}$  shown here and a corresponding increase  
278 in nitrate utilisation (Figure 5A). Our calculations of  $\text{Si}(\text{OH})_4 \text{ supply}$  show the supply of silicic acid to  
279 the photic zone over this period is extremely variable (2.53-2.63 Ma) and shows distinct peaks  
280 compared to the levels experienced prior to NHG (Figure 5A), which suggests that changes in  
281 supply of silicic acid may be driving the changes in  $\% \text{Si}(\text{OH})_4 \text{ utilisation}$  at this time, rather than Fe  
282 limitation. Our data suggests that the general decrease in silicic acid utilisation is accompanied by  
283 a variable but significant increase in  $\text{Si}(\text{OH})_4 \text{ supply}$ , although the source of this is not clear. Previous  
284 work has discussed the role of ice sheets on the global silicon cycle and suggested that ice sheets  
285 could have delivered large quantities of isotopically light silica to the oceans during periods of

286 enhanced glacial activity (Hawkings et al., 2017). At the same time, large fluctuations in  $\delta^{18}\text{O}_{\text{diatom}}$   
287 of c. 5 ‰ at 2.67 Ma are attributed to freshwater input from glacial meltwater (Swann, 2010),  
288 suggesting the enhanced peaks in  $\text{Si(OH)}_4$  supply may originate from the same glacial source.

289

290 The large changes in the supply of silicic acid to the photic zone and variable (although declining)  
291  $\%\text{Si(OH)}_4$  utilisation, variable  $\delta^{15}\text{N}$ , accompanied by an increase in BSi (%wt), following the initial crash  
292 at 2.73 Ma would indicate potential differences in water column conditions. There is an evident  
293 influx of meltwater as indicated by the changes in  $\delta^{18}\text{O}_{\text{diatom}}$ , and potentially  $\text{Si(OH)}_4$  supply as well as  
294 some form of nutrient limitation affecting  $\%\text{Si(OH)}_4$  utilisation nitrate utilisation, although these  
295 changes are not synchronous (Figure 5A). By 2.48 Ma, there is a return to complete utilisation of  
296 silicic acid and a drop in silicic acid supply, indicating a more established stratified ocean. Between  
297 2.40-2.48 Ma there is a significant freshening to the photic zone, indicated by a > 8 ‰ drop in  
298  $\delta^{18}\text{O}_{\text{diatom}}$ , accompanied by a drop in opal productivity from 40% to close to zero and enhanced ice-  
299 rafted debris IRD deposition (Bailey et al., 2011), which could relate to a further intensification of  
300 NHG, similar to 2.73 Ma. By 2.28 Ma  $\delta^{18}\text{O}_{\text{diatom}}$  has increased by > 10 ‰ (Figure 5A) to levels  
301 similar to the Pliocene and suggests a decreased input of meltwater at a time of enhanced  
302 nutrient utilisation under a relatively reduced supply. It has previously been suggested that the  
303 region acted as a net sink for  $\text{CO}_2$  following NHG and the formation of the halocline (Swann et al.,  
304 2018). The changes in our  $\%\text{Si(OH)}_4$  supply and  $\%\text{Si(OH)}_4$  utilisation data over this period however,  
305 suggests variable efficiency in the biological pump at a time of instability in palaeoceanographic  
306 conditions, given the dramatic changes in  $\delta^{18}\text{O}_{\text{diatom}}$ , (Figure 5A).

307

308 **4.2 Middle Quaternary and the MPT**

309 In the middle Quaternary, prior to the MPT (1.38-1.64 Ma Figure 5B), there is significant variation  
310 in siliceous productivity, silicic acid supply and utilisation. Our results show reduced consumption  
311 of nutrients is linked to both enhanced and reduced nutrient supply but predominantly generally  
312 low productivity. Over MIS 51-52 (1.51-1.53 Ma) utilisation is high yet opal productivity varies  
313 significantly (between 5 and 66%). Our supply data indicates an increase in the supply of nutrients  
314 during the interglacial (MIS 51), corresponding to a productivity peak (Figure 5B). Complete  
315 consumption of nutrients at times of enhanced productivity and nutrient supply would be similar  
316 to pre-NHG times when there was unimpeded deep water upwelling, as has been suggested for  
317 more recent records from this area (MIS 5b/c: Swann and Snelling, 2015, MIS 2 Okazaki et al.,  
318 2010).

319

320 Our  $\delta^{30}\text{Si}_{\text{diatom}}$  record and associated utilisation and supply data over the MPT are not noticeably  
321 different to the Early Quaternary in terms of variability, however the inter-relationships between  
322 productivity, supply and utilisation of nutrients does vary as discussed below. There are two  
323 distinct excursions in the nutrient utilisation record (1.54-1.60 Ma and 0.93-1.0 Ma), and  
324 productivity and supply are slightly enhanced over this period, such that mean opal wt% = 26%  
325 over the MPT and 13% pre-MPT. At the onset of the MPT, 1.25 Ma, productivity and nutrient  
326 supply are enhanced, whilst utilisation is slightly reduced and  $\delta^{18}\text{O}_{\text{diatom}}$  is at similar levels to the  
327 Pliocene (Figure 5B). Reduced utilisation during periods of increased supply have previously been  
328 linked in part to iron flux contributing to nutrient limitation (Bailey et al., 2011). Here, the scale of  
329 change compared to the period immediately following the onset of NHG, however, is much  
330 smaller and short lived. Worne et al., (2020) have indicated reduced upwelling over the MPT in the  
331 Bering Sea, controlled by sea ice extent and the expansion of GNPIW into the wider subarctic  
332 region and that prior to the middle MPT (0.9 Ma) other/additional factors were controlling

333 nutrient upwelling. The enhanced nutrient supply and productivity reported here suggest GNPIW  
334 may not have reached this far south at this time and that nutrient supply may have been more  
335 affected by a reduction in the strength of the halocline. The reduced utilisation under such  
336 conditions would indicate a less efficient biological pump.

337

338 Following the initial MPT opal high, our record shows a decrease in productivity and silicon supply,  
339 coupled with 4.4‰ drop in  $\delta^{18}\text{O}_{\text{diatom}}$  and a rise in nutrient utilisation (1.24-1.16 Ma, MIS 37-35)  
340 (Figure 5B). It has previously been discussed that large changes in  $\delta^{18}\text{O}_{\text{diatom}}$  are indicative of a  
341 freshening from meltwater and precipitation that could affect stratification and prevent upwelling  
342 of deeper water and thus nutrients. This could have led to a return to stratified conditions  
343 (halocline and potentially GNPIW) with complete utilisation of the available nutrients. It is also at  
344 this time that there is an evident change in the LR04 record (Lisecki and Raymo 2005) transitioning  
345 to 100 kyr cycles becoming more evident.

346

347 This pattern of enhanced supply and productivity and reduced utilisation, prior to a drop in  
348  $\delta^{18}\text{O}_{\text{diatom}}$  is similar to the period in the early Quaternary, where it was suggested that  
349 palaeoceanographic conditions may have been more unstable and the role of glacial meltwater  
350 could have had an effect on the supply of nutrients to the photic zone. The variability at this time  
351 is less pronounced than earlier in the Quaternary and could indicate that any weakening in the  
352 halocline was minimal and/or short lived.

353

354 The modern day halocline is preserved through high precipitation and low evaporation (Emile-  
355 Geay et al., 2003) but it is unlikely that the freshening at MIS 37-35 is solely a result of increased  
356 precipitation. Freshwater input to the surface waters could also be a result of glacial melt water,

357 which for this region is likely to originate from the Bering Sea (Swann 2010, Kotilainen and  
358 Shackleton, 1995; McKelvey et al., 1995; St John and Krissek, 1999) as there is a pronounced  
359 seasonal advance and retreat of sea ice at this time (Detlef et al., 2018). It is possible that there  
360 were other sources of meltwater to this region including the Sea of Okhotsk, where proxy records  
361 indicate similarities in sea surface temperature change to the North Pacific (Lattaud et al., 2019)  
362 and the Kamchatka-Koryak coast which has been suggested as a source of meltwater to this area  
363 for the Late Quaternary (McCarron et al., 2021). IRD records from the Sea of Okhotsk suggest  
364 however, that it is a less likely source (McKelvey et al., 1995; St John and Krissek, 1999). Lam et  
365 al. (2013) showed from various proxy records that there was a productivity peak in the North  
366 Pacific at 14.5 kyr following deglaciation, with a subsequent freshening of surface waters,  
367 enhancing stratification in the upper ocean waters due to shutting down of relatively deep ocean  
368 convection. Swann and Snelling (2015) however show that freshwater acts as a secondary control  
369 on re-establishing ocean stratification and suggest that other factors including linkages to the  
370 Southern Ocean could be driving ocean stratification (Jaccard et al., 2005, 2010, Sigman et al.,  
371 2010, 2021. We are unable to discern whether the freshwater input is a primary or secondary  
372 factor affecting upwelling at this time.

373

374 The upwelling index from the Bering Sea indicates an upwelling high in the middle of MIS 35, whilst  
375 our productivity and supply in the subarctic Pacific are in general decline following peaks in  
376 productivity in the preceding interglacial (MIS 37). There is no available upwelling data for MIS 37,  
377 but for MIS 35 it would suggest that there were different controls influencing upwelling between  
378 the two regions and that Bering Sea meltwater was not acting as a major influence on upwelling in  
379 the North Pacific Ocean at this time. The decrease in productivity over MIS 37-35 recorded in our  
380 data is in contrast to the findings of Diester-Haas et al. (2018), where an increase in productivity is



381 linked to (but not driving) the sequestration of CO<sub>2</sub>. The decrease in our proxy data is of a similar  
382 magnitude to conditions at the onset of NHG for the North Pacific (Haug, 1995, Reynolds et al.,  
383 2008, Swann, 2010, Bailey et al., 2011) and the formation of the halocline. Over MIS 37-35, our  
384 data highlights the sensitivity of the North Pacific region to stratification, which we suggest occurs  
385 at this time.

386

387 From 1-0.9 Ma (MIS 30-23), productivity is highly variable and shows no link to glacial/interglacial  
388 cycles. Utilisation is also variable, but enhanced supply of nutrients is often associated with high  
389 productivity. Low utilisation is associated with moderate to enhanced supply of nutrients and  
390 productivity over both glacial and interglacial cycles. Compared to the Bering Sea upwelling index,  
391 our productivity and supply data show some broad similarities, suggesting that GNPIW may be  
392 having more of an influence on North Pacific Ocean stratification at this time. This may be linked  
393 to closure of the Bering Strait (Kender et al., 2018, Worne et al., 2019, 2020,) and an increase in  
394 sea ice extent, which may have forced a greater link with the North Pacific Ocean.

395

### 396 **4.3 Late Quaternary records**

397 From the end of the MPT (0.7 Ma) to 0.48 Ma (MIS 18-13 Figure 5C) productivity peaks are  
398 predominantly associated with interglacials and enhanced supply but irregular consumption. In  
399 addition, productivity peaks are more closely aligned with the Bering Sea upwelling index (Worne  
400 et al., 2019), suggesting GNPIW during glacial periods in the North Pacific Ocean and upwelling  
401 during interglacial periods and an apparent link between climate change and productivity across  
402 the North Pacific region.

403

404 Records from 0.2-0.06 Ma (MIS 7-4 Figure 5D) show a greater range of variability in nutrient  
405 supply and utilisation than over the MPT, accompanied by a significant oceanic freshening (Swann  
406 and Snelling, 2015), which is suggested to have a strong influence on ocean stratification and the  
407 strength of the halocline. Nutrient productivity and supply appear to correspond with the Bering  
408 Sea upwelling index, indicating a continued alignment between the Bering Sea and the wider  
409 North Pacific region. Previous studies have indicated a strong link between the biogeochemistry of  
410 the North Pacific Ocean and climate (Jaccard et al., 2010, Knudson and Ravelo 2015b, Worne et al.,  
411 2020) and that the opening/closing of the Bering Strait would have had a strong influence on the  
412 formation of GNPIW, following the MPT (Worne et al., 2020).

413

## 414 **5. Conclusions**

415 Over the analysed interval our proxy data suggests that the North Pacific Ocean may have  
416 undergone changes in the strength of the ocean stratification throughout the Quaternary period  
417 as a result of weakening in the halocline and/or influence of GNPIW/NPIW. A number of factors  
418 likely influenced the changing ocean state, to varying degrees, over time however it would appear  
419 that prior to MIS 21, climate change and glacial-interglacial cycles were not driving productivity  
420 changes in this region and that factors influencing the Bering Sea did not impact the North Pacific  
421 Region in the same way. Between MIS 21-13 and MIS 7-4, climate and the influences of GNPIW did  
422 affect the North Pacific Ocean state, indicating a greater influence from the Bering Sea region.

423

424 Nutrient use and supply also do not appear to have been driven by climate change but are  
425 influenced by other factors that we are unable to quantify from our data. They do however show  
426 periods of a highly efficient biological pump (high productivity, high supply, complete  
427 consumption), which would have reduced any exchange of CO<sub>2</sub> with the atmosphere and may

428 have served to sequester CO<sub>2</sub> deep in the ocean. Our data also show periods of inefficiency (high  
429 productivity, high supply, incomplete consumption) when the region may have acted as a source  
430 of CO<sub>2</sub> to the atmosphere. These periods of lower consumption in periods of higher productivity  
431 and supply require further investigation along with other proxy evidence. Modelling experiments  
432 have shown that a breakdown in stratification in the North Pacific is capable of producing a 30  
433 ppm rise in atmospheric CO<sub>2</sub> (Rae et al., 2014). This is not insignificant and if a breakdown in  
434 stratification was more of a regular feature in the North Pacific Ocean over the Quaternary, then  
435 the role of this region in regulating global climate may have been previously underestimated and  
436 requires further clarification.

437

#### 438 **Acknowledgements**

439 This research was funded through a Daphne Jackson Research Fellowship for AS (2017-2019). The  
440  $\delta^{30}\text{Si}$  and  $\delta^{18}\text{O}$  analyses were completed through funding provided by the NERC Isotope  
441 Geosciences Facilities Steering Committee grant IP-1786-1117 (to GEAS). We are grateful to the  
442 International Ocean Discovery Program, including the crew on ODP Leg 145 for collecting the  
443 samples from Site 882 and the Texas Core Repository curators. AS completed all of the sample  
444 preparation, ran the  $\delta^{30}\text{Si}$  analysis with VP and led the writing of the manuscript. JL ran the  
445 analysis of  $\delta^{18}\text{O}$  on prepared sample material. All authors contributed to the writing and  
446 interpretation of the manuscript.

447

448

449

450

451

452

453

454

455

456

457 **References**

458 Bailey, I., Q. Liu, G. E. A. Swann, Z. Jiang, Y. Sun, X. Zhao, and A. P. Roberts 2011, Iron fertilisation  
459 and biogeochemical cycles in the sub-Arctic northwest Pacific during the late Pliocene  
460 intensification of Northern Hemisphere glaciation, *Earth Planet. Sci. Lett.*, 307(3–4), 253–265,  
461 doi:10.1016/j.epsl.2011.05.029

462

463 Brandriss, M. E., O’Neil, J. R., Edlund, M. B., and Stoermer, E. F. 1998, Oxygen isotope fractionation  
464 between diatomaceous silica and water, *Geochim. Cosmochim. Ac.*, 62, 1119–1125.

465

466 Brunelle, B. G., Sigman, D. M., Jaccard, S. L., Keigwin, L. D., Plessen, B., Schettler, G., Cook, M. S.,  
467 and Haug, G. H. 2010, Glacial/interglacial changes in nutrient supply and stratification  
468 in the western subarctic North Pacific since the penultimate glacial maximum, *Quaternary Sci.*  
469 *Rev.*, 29, 2579–2590.

470

471 Cassarino, L., Coath, C.D., Xavier, J. R., and Hendry, K. R. 2018, Silicon isotopes of deep sea  
472 sponges: new insights into biomineralisation and skeletal structure *Biogeosciences*, 15 (22).

473

474 Clark, P.U., Pollard, D., 1998. Origin of the middle Pleistocene transition by ice sheet  
475 erosion of regolith. *Paleoceanography* 13, 1–9.

476

477 Cockerton, H.E., Street-Perrott, F.A., Leng, M.J., Barker, P.A., Horstwood, M.S.A., Pashley, V., 2013.  
478 Stable-isotope (H, O, and Si) evidence for seasonal variations in hydrology and Si cycling from  
479 modern waters in the Nile Basin: implications for interpreting the Quaternary record. *Quaternary*  
480 *Science Reviews* 66, 4–21.

481

482 Cortese, G., R. Gersonde, C.-D. Hillenbrand, and G. Kuhn, 2004, Opal sedimentation shifts in the  
483 World Ocean over the last 15 Myr, *Earth Planet. Sci. Lett.*, 224, 509–527

484

485 Crowley, T.J., Hyde, W.T., 2008. Transient nature of late Pleistocene climate variability.  
486 *Nature* 456, 226–230.

487

488 de La Rocha, C.L., Brzezinski, M.A., DeNiro, M.J., 1997. Fractionation of silicon isotopes by marine  
489 diatoms during biogenic silica formation. *Geochim. Cosmochim. Acta* 61, 5051–5056.

490

491 de la Rocha, C. L. 2003, Silicon isotope fractionation by marine sponges and the reconstruction of  
492 the silicon isotope composition of ancient deep water, *Geology*, 31, 423–426.

493

494 Detlef, H., Belt, S.T., Sosdian, S.M., Smik, L., Lear, C.H., Hall, I.R., Cabedo-Sanz, P., Husum, K.,  
495 Kender, S., 2018. Sea ice dynamics across the Mid-Pleistocene transition in the Bering Sea. *Nat.*  
496 *Commun.*9. <https://doi.org/10.1038/s41467-018-02845-5>.

497

498 Diester-Haass, L., Billups, K., Lear, C., 2018, Earth-science reviews productivity changes across the  
499 mid-Pleistocene climate transition *Earth-Sci. Rev.*, 179, pp. 372-

500 391, [10.1016/j.earscirev.2018.02.016](https://doi.org/10.1016/j.earscirev.2018.02.016)

501

502 Emile-Geay, J., Cane, M. A., Naik, N., Seager, R., Clement, A. C., and van Green, A. 2003, Warren  
503 revisited: atmospheric freshwater fluxes and “Why is no deep water formed in the North Pacific”,  
504 *J. Geophys. Res.*, 108, 3178, doi:10.1029/2001JC001058.

505

506 Galbraith, E.D., Jaccard, S.L., Pedersen, T.F., Sigman, D.M., Haug, G.H., Cook, M., Southon, J.R.,  
507 Francois, R., 2007. Carbon dioxide release from the North Pacific abyss during the last deglaciation.  
508 *Nature* 449, 890–893. <https://doi.org/10.1038/nature06227>.

509

510 Galbraith, E.D., Kienast, M., Jaccard, S.L., Pedersen, T.F., Brunelle, B.D., Sigman, D.M., Kiefer, T.,  
511 2008. Consistent relationship between global climate and surface nitrate utilisation in the  
512 western subarctic Pacific throughout the last 500 ka. *Paleoceanography* 23, 1–11. [https://doi.org](https://doi.org/10.1029/2007PA001518)  
513 [/10.1029/2007PA001518](https://doi.org/10.1029/2007PA001518).

514

515 Gebhardt, H., Sarnthein, M., Grootes, P. M., Kiefer, T., Kuehn, H., Schmieder, F., and Rohl, U. 2008  
516 Paleonutrient and productivity records from the subarctic North Pacific for Pleistocene  
517 glacial terminations I to V, *Paleoceanography*, 23, PA4212, doi:10.1029/2007PA001513.

518

519 Gong, X., Lembke-Jene, L., Lohmann, G., Knorr, G., Tiedemann, R., Zou, J. J., Shi, X. F. 2019  
520 Enhanced North Pacific deep-ocean stratification by stronger intermediate water formation during  
521 Heinrich Stadial 1. *Nat Commun* 10, 656. <https://doi.org/10.1038/s41467-019-08606-2>

522

523 Gray, W.R., Rae, J.W.B., Wills, R.C.J., Shevenell, A.E., Taylor, B., Burke, A., Foster, G.L., Lear, C.H.,  
524 2018. Deglacial upwelling, productivity and CO<sub>2</sub> outgassing in the North Pacific Ocean. *Nat.*  
525 *Geosci.* 11, 340–344. <https://doi.org/10.1038/s41561-018-0108-6>.

526

527 Haug, G.H., Maslin, M.A., Sarnthein, M., Stax, R., Tiedemann, R., 1995. Evolution of  
528 northwest Pacific sedimentation patterns since 6 Ma (Site 882). In: Rea, D.K.,

- 529 Basov, I.A., Scholl, D.W., Allan, J.F. (Eds.), Proceedings of the Ocean Drilling Program.  
530 Scientific Results. Ocean Drilling Program, College Station, TX, pp. 293–314.  
531
- 532 Haug, G. H., D. M. Sigman, R. Tiedemann, T. F. Pedersen, and M. Sarnthein, 1999, Onset of  
533 permanent stratification in the subarctic Pacific Ocean, *Nature*, 401, 779–782.  
534
- 535 Haug, G. H., Ganopolski, A., Sigman, D. M., Rosell-Mele, A., Swann, G. E. A., Tiedemann, R.,  
536 Jaccard, S, Bollmann, J., Maslin, M. A., Leng, M. J., and Eglinton, G. 2005 North Pacific seasonality  
537 and the glaciation of North America 2.7 million years ago, *Nature*, 433, 821–825.  
538
- 539 Horikawa, K., Asahara, Y., Yamamoto, K., Okazaki, Y., 2010. Intermediate water formation in the  
540 Bering Sea during glacial periods: evidence from neodymium isotope ratios. *Geology*38, 435–438.  
541 <https://doi.org/10.1130/G30225.1>.  
542
- 543 Horn, M. G., C. P. Beucher, R. S. Robinson, and M. A. Brzezinski., 2011, Southern ocean nitrogen  
544 and silicon dynamics during the last deglaciation, *Earth Planet. Sci. Lett.*, 310, 334–339.  
545
- 546 Jaccard, S. L., Haug, G. H., Sigman, D. M., Pedersen, T. F., Thierstein, H. R., and Röhl, U. 2005,  
547 Glacial/interglacial changes in subarctic North Pacific stratification, *Science*, 308, 1003–1006.  
548
- 549 Jaccard, S. L., Galbraith, E. D., Sigman, D. M., Haug, G. H., Francois, R., Pedersen, T. F., Dulski, P.,  
550 and Thierstein, H. R. 2009, Subarctic Pacific evidence for a glacial deepening of the oceanic  
551 respired carbon pool, *Earth Planet. Sc. Lett.*, 277, 156–165.  
552



- 553 Jaccard, S. L., E. D. Galbraith, D. M. Sigman, and G. H. Haug, 2010, A pervasive link between  
554 Antarctic ice core and subarctic Pacific sediment records over the past 800 kyrs, *Quat. Sci. Rev.*,  
555 29(1–2), 206–212, doi:10.1016/j.quascirev.2009.10.007.  
556
- 557 Jang, K., Huh, Y., Han, Y., 2017, Authigenic Nd isotope record of North Pacific In-termediate Water  
558 formation and boundary exchange on the Bering Slope. *Quat. Sci. Rev.*156, 150–163.  
559 <https://doi.org/10.1016/j.quascirev.2016.11.032>.  
560
- 561 Katsura, S., H. Ueno, H. Mitsudera, and S. Kouketsu, 2020: Spatial distribution and seasonality of  
562 halocline structures in the subarctic North Pacific. *J. Phys. Oceanogr.*, **50**, 95–  
563 109, <https://doi.org/10.1175/JPO-D-19-0133.1>.  
564
- 565 Kender, S., Ravelo, A.C., Worne, S., Swann, G.E.A., Leng, M.J., Asahi, H., Becker, J., Detlef, H., Aiello,  
566 I.W., Andreasen, D., Hall, I.R., 2018. Closure of the Bering strait caused mid-Pleistocene transition  
567 cooling. *Nat. Commun.* 9. <https://doi.org/10.1038/s41467-018-07828-0>  
568
- 569 Kohfeld, K. E. and Chase, Z. 2011 Controls on deglacial changes in biogenic fluxes in the North  
570 Pacific Ocean, *Quaternary Sci. Rev.*, 30, 3350–3363.  
571
- 572 Knudson, K.P., Ravelo, A.C., 2015a. North Pacific Intermediate Water circulation enhanced by the  
573 closure of the Bering Strait. *Paleoceanography*30, 1287–1304. <https://doi.org/10.1002/2015PA002840>.  
574  
575

- 576 Knudson, K and Ravelo A. C. 2015b Enhanced Subarctic Pacific Stratification and nutrient utilisation  
577 during glacials over the last 1.2 Myr *Geophysical Research Letters* 42 9870-9879  
578
- 579 Kotilainen, A.T., Shackleton, N.J., 1995. Rapid climate variability in the North Pacific  
580 Ocean during the past 95,000 years. *Nature* 377, 323–326.  
581
- 582 Lam, P. J., Robinson, L. F., Blusztajn, J., Li, C., Cook, M. S., McManus, J. F., and Keigwin, L. D. 2013,  
583 Transient stratification as the cause of the North Pacific productivity spike during deglaciation,  
584 *Nat. Geosci.*, 6, 622–626, 2013.  
585
- 586 Lattaud, J., Lo, L., Zeeden, C., Liu, Y.J., Song, S.R., van der Meer, M.T.J., Sinninghe Damsté,  
587 J.S., Schouten, S. 2019, A multiproxy study of past environmental changes in the Sea of Okhotsk  
588 during the last 1.5 Ma *Org Geochem.*, 132, pp. 50-61  
589
- 590 Lee, S.-Y., Poulsen, C.J., 2006. Sea ice control of Plio-Pleistocene tropical Pacific climate  
591 evolution. *Earth and Planetary Science Letters* 248, 238–247.  
592
- 593 Lisiecki, L.E., Raymo, M.E., 2005. A Pliocene–Pleistocene stack of 57 globally distributed  
594 benthic  $\delta^{18}O$  records. *Paleoceanography* 20, PA1003. [http://dx.doi.org/10.1029/](http://dx.doi.org/10.1029/2004PA001071)  
595 [2004PA001071](http://dx.doi.org/10.1029/2004PA001071).  
596
- 597 Max, L., Lembke-Jene, L., Riethdorf, J.R., Tiedemann, R., Nürnberg, D., Kühn, H., MacKensen, A.,  
598 2014. Pulses of enhanced north Pacific intermediate water ventilation from the Okhotsk Sea and

599 Bering Sea during the last deglaciation. *Clim. Past*10, 591–605. [https://doi.org/10.5194/cp-10-](https://doi.org/10.5194/cp-10-591-2014)  
600 591-2014.  
601  
602 McCarron, A.P., Bigg, G.R., Brooks, H., Leng, M.J., Marshall, J.D., Ponomareva, V., Portnyagin, M.,  
603 Reimer, J., Rogerson, M., 2021, Northwest Pacific ice-rafted debris at 38°N reveals episodic ice-  
604 sheet change in late Quaternary Northeast Siberia. *Earth and Planetary Science letters* 553  
605 <https://doi.org/10.1016/j.epsl.2020.116650>  
606  
607 McClymont, E.L., Rosell-Melé, A., 2005. Links between the onset of modern Walker Circulation and  
608 the mid-Pleistocene climate transition. *Geology* 33, 389–392.  
609  
610 McClymont, E.L., Sosdian, S.M., Rosell-Melé, A., Rosenthal, Y., 2013. Pleistocene sea-surface  
611 temperature evolution: early cooling, delayed glacial intensification, and implications for the mid-  
612 Pleistocene climate transition. *Earth-Sci. Rev.*123, 173–193. [https://doi.org/10.1016/j](https://doi.org/10.1016/j.earscirev.2013.04.006)  
613 [.earscirev.2013.04.006](https://doi.org/10.1016/j.earscirev.2013.04.006). McKelvey et al 1995.  
614  
615 Moschen, R., Lücke, A., Schleser, G., 2005. Sensitivity of biogenic silica oxygen isotopes  
616 to changes in surface water temperature and palaeoclimatology. *Geophys. Res. Lett.*  
617 32, L07708. doi:10.1029/2004GL022167.  
618  
619 Nelson, D.M., Treguer, P., Brzezinski, M.A., Leynaert, A., Queguiner, B. 1995 Production and  
620 dissolution of biogenic silica in the ocean: revised global estimates, comparison with regional data  
621 and relationship to biogenic sedimentation *Global Biogeochem. Cycles*, 9, pp. 359-372.  
622

- 623 Otosaka, S., and S. Noriki, 2005, Relationship between composition of settling particles and  
624 organic carbon flux in the western North Pacific and the Japan Sea, *J. Oceanogr.*, **61**(1), 25–40.  
625
- 626 Panizzo, V.N., Swann, G.E.A., Mackay, A.W., Vologina, E., Sturm, M., Pashley, V., Horstwood,  
627 M.S.A., 2016. Insights into the transfer of silicon isotopes into the sediment record. *Biogeosciences*  
628 **13**, 147–157.  
629
- 630 Rae, James, Gray, William, Inglin Wills, Robert, Eisenman, Ian, Fitzhugh, Ben, Fotheringham,  
631 Morag, Littley, Eloise, Rafter, Patrick, Rees-Owen, Rhian, Ridgewell, Andrew, Taylor, Ben, Burke,  
632 Andrea. 2020, Overturning circulation, nutrient limitation, and warming in the Glacial North  
633 Pacific. *Science Advances*. **6**. eabd1654. 10.1126/sciadv.abd1654.  
634
- 635 Rae, J. W. B., Sarthein, M., Foster, G. L., Ridgwell, A., Grootes, P. M., and Elliott, T. 2014, Deep  
636 water formation in the North Pacific and deglacial CO<sub>2</sub> rise, *Paleoceanography*, **29**, 645–667,  
637 2014.  
638
- 639 Ravelo, A.C., Andreasen, D.H., Lyle, M., Olivarez Lyle, A., Wara, M.W., 2004. Regional climate  
640 shifts caused by gradual global cooling in the Pliocene epoch. *Nature* **429**, 263–267.  
641
- 642 Raymo, M.E., 1997. The timing of major climate terminations. *Paleoceanography* **12**,  
643 577–585.  
644
- 645 Raymo, M.E., Lisiecki, L.E., Nisancioglu, K.H., 2006. Plio-Pleistocene ice volume, Antarctic  
646 climate, and the global  $\delta^{18}O$  record. *Science* **313**, 492–495. Reynolds et al 2008

- 647 Reynolds, B. C. 2009, Modeling the modern marine  $\delta^{30}\text{Si}$  distribution, *Global Biogeochem. Cycles*,  
648 23, GB2015, doi:10.1029/2008GB003266.
- 649
- 650 Sarnthein, M., Gebhardt, H., Kiefer, T., Kucera, M., Cook, M., and Erlenkeuser, H. 2004, Mid  
651 Holocene origin of the sea-surface salinity low in the subarctic North Pacific, *Quaternary Sci. Rev.*,  
652 23, 2089–2099.
- 653
- 654 Shcherbina, A. Y.; L. D. Talley and D. L. Rudnick. 2003. Direct observations of North Pacific  
655 ventilation: Brine rejection in the Okhotsk Sea. *Science*, 302: 1952–1955.
- 656
- 657 Sigman, D. M. & Hain, M. P. 2012, The Biological Productivity of the Ocean: Section 2. *Nature*  
658 *Education Knowledge* 3(10):20
- 659
- 660 Sigman, D. M., Hain, M. P., & Haug, G. H. 2010. The polar ocean and glacial cycles in atmospheric  
661 CO<sub>2</sub> concentration. *Nature*, 466(7302), 47–55. <https://doi.org/10.1038/nature09149>
- 662
- 663 Sigman, D. M., Fripiat, F., Studer, A. S., Kemeny, P. C., Martínez-García, A., Hain, M. P., Ai, X.,  
664 Wang, X., ren, H., Haug, G. 2021. The Southern Ocean during the ice ages: A review of the  
665 Antarctic surface isolation hypothesis, with comparison to the North Pacific. *Quaternary Science*  
666 *Reviews*, 254,  
667 106732
- 668
- 669 Sigman, D. M., Jaccard, S. L., & Haug, G. H. 2004. Polar ocean stratification in a cold climate.  
670 *Nature*, 428(6978), 59–63. <https://doi.org/10.1038/nature02357>

671

672 Smetacek, V. Diatoms and the ocean carbon cycle. *Protists* **150**, 25–32 1999.

673

674 St John, K.E.K., Krissek, L.A., 1999. Regional patterns of Pleistocene ice-rafted debris flux  
675 in the North Pacific. *Paleoceanography* **14**, 653–662.

676

677 Swann, G. E. A. 2010, Salinity changes in the North West Pacific Ocean during the late  
678 Pliocene/early Quaternary from 2.73 Ma to 2.53 Ma, *Earth Planet. Sc. Lett.*, **297**, 332–338.

679

680 Swann, G. E. A., Snelling, A. M., & Pike, J., 2016. Biogeochemical cycling in the Bering Sea over the  
681 onset of major Northern Hemisphere glaciation. *Paleoceanography*, **31**, 1261–1269.

682 <https://doi.org/10.1002/2016PA002978>.

683

684 Swann, G.E.A.; Snelling, A.M. 2015 Photic zone changes in the north-west Pacific Ocean from MIS  
685 4–5e. *Climate of the Past*, **11** (1). 15–25. <https://doi.org/10.5194/cp-11-15-2015>

686

687 Swann, G.E.A., Kendrick, C.P., Dickson, A.J. and Worne, S., 2018. [Late Pliocene marine pCO<sub>2</sub>](#)  
688 [reconstructions from the Subarctic Pacific Ocean](#) *Paleoceanography and*

689 *Paleoclimatology*. **33**, 457–469

690

691 Tiedemann, R., and Haug, G. H., 1995, Astronomical calibration of cycle stratigraphy for Site 882 in  
692 the northwest Pacific, *Proc. Ocean Drill. Program Sci. Results*, **145**, 283–292.

693

694 Tsuda, A., Takeda, S., Saito, H., Nishioka, J., Nojiri, Y., Kudo, I., Kiyosawa, H., Shiimoto, A.,

- 695 Imai, K., Ono, T., Shimamoto, A., Tsumune, D., Yoshimura, T., Aono, T., Hinuma, A.,  
696 Kinugasa, M., Suzuki, K., Sohrin, Y., Noiri, Y., Tani, H., Deguchi, Y., Tsurushima, N.,  
697 Ogawa, H., Fukami, K., Kuma, K., Saino, T., 2003. A mesoscale iron enrichment in the  
698 Western Subarctic Pacific induces a large centric diatombloom. *Science* 300, 958–961.  
699  
700 Tziperman, E., Gildor, H., 2003. On the mid-Pleistocene transition to 100-ky glacial cycles  
701 and the asymmetry between glaciation and deglaciation times. *Paleoceanography* 18,  
702 1–8.  
703  
704 Volk, T. & Hoffert, M. I. 1985, in *The Carbon Cycle and Atmospheric CO<sub>2</sub>: Natural Variation*  
705 *Archean to Present* (eds E. T. Sundquist, E. T. & Broecker, W. S.) (AGU Monograph 32, American  
706 Geophysical Union, Washington DC).  
707  
708 Wang, Y., Zhang, H., Chen, H., & Chai, F., 2019 The sources and transport of iron in the North  
709 Pacific and its impact on marine ecosystems, *Atmospheric and Oceanic Science Letters*, 12:1, 30-  
710 34, DOI: [10.1080/16742834.2019.1545513](https://doi.org/10.1080/16742834.2019.1545513)  
711  
712 M.J. Warner, G.I. Roden, 1995 Chlorofluorocarbon evidence for recent ventilation of the deep  
713 Bering Sea Nature, 373, pp. 409-412.  
714  
715 Worne, S., Kender, S., Swann, G.E.A., Leng, M.J., and Ravello, A.C., 2019. Coupled climate and  
716 subarctic Pacific nutrient upwelling over the last 850,000 years. *Earth and Planetary Science*  
717 *Letters*. 522, 87 – 97.  
718

719 Worne, S., Kender, S., Swann, G.E.A., Leng, M.J., and Ravello, A.C., 2020, Reduced upwelling of  
720 nutrient and carbon-rich water in the subarctic Pacific during the Mid-Pleistocene Transition.

721 *Palaeogeography, Palaeoclimatology, Palaeoecology* 555

722 <https://doi.org/10.1016/j.palaeo.2020.109845>

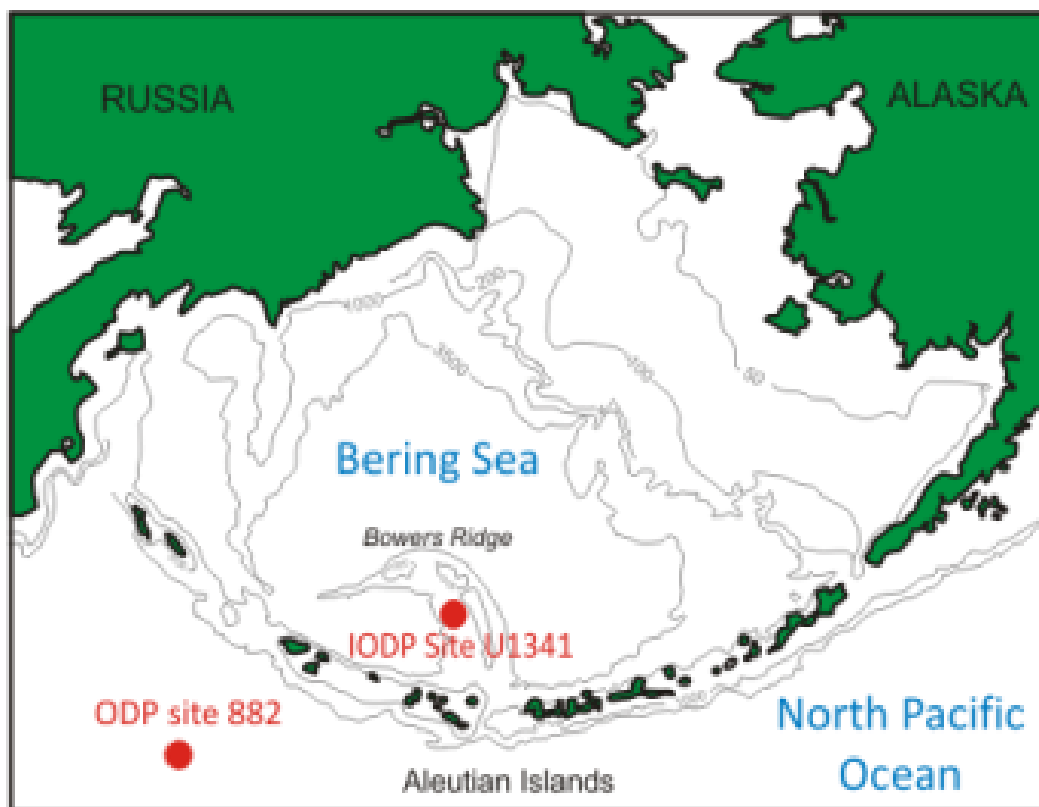
723

724

725



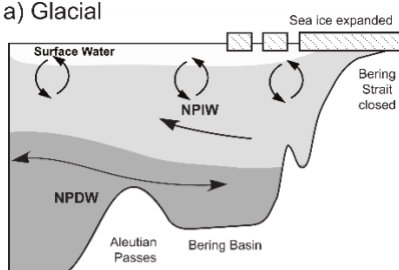
726 Figures



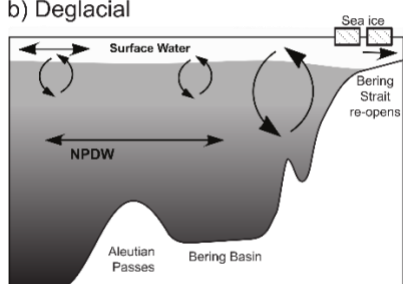
727

728 Figure 1 [colour]: Location of ODP Site 882 and IODP Site 1341.

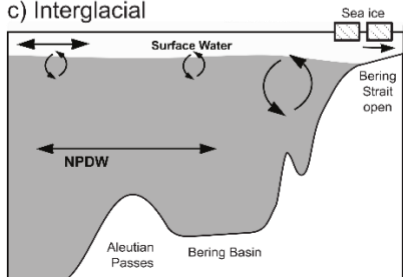
a) Glacial



b) Deglacial



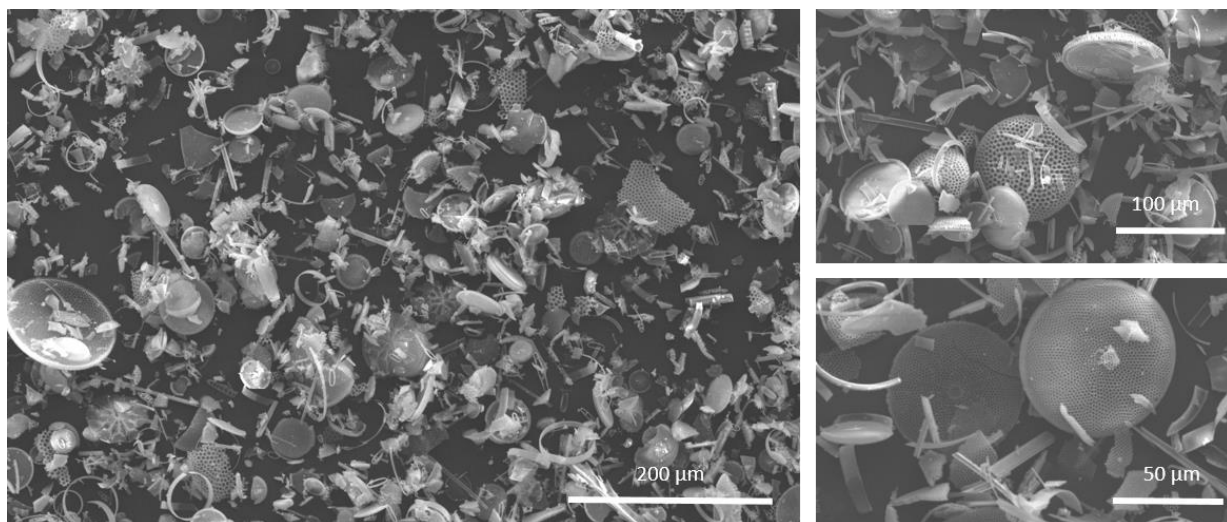
c) Interglacial



729

730 Figure 2: Schematic models representing Late Quaternary glacial, deglacial and interglacial  
731 biogeochemical cycling between the Bering Sea and the North Pacific Ocean and the propagation  
732 of southwards GNPIW. Modified from Kender et al 2018 and Worne et al 2019.

733

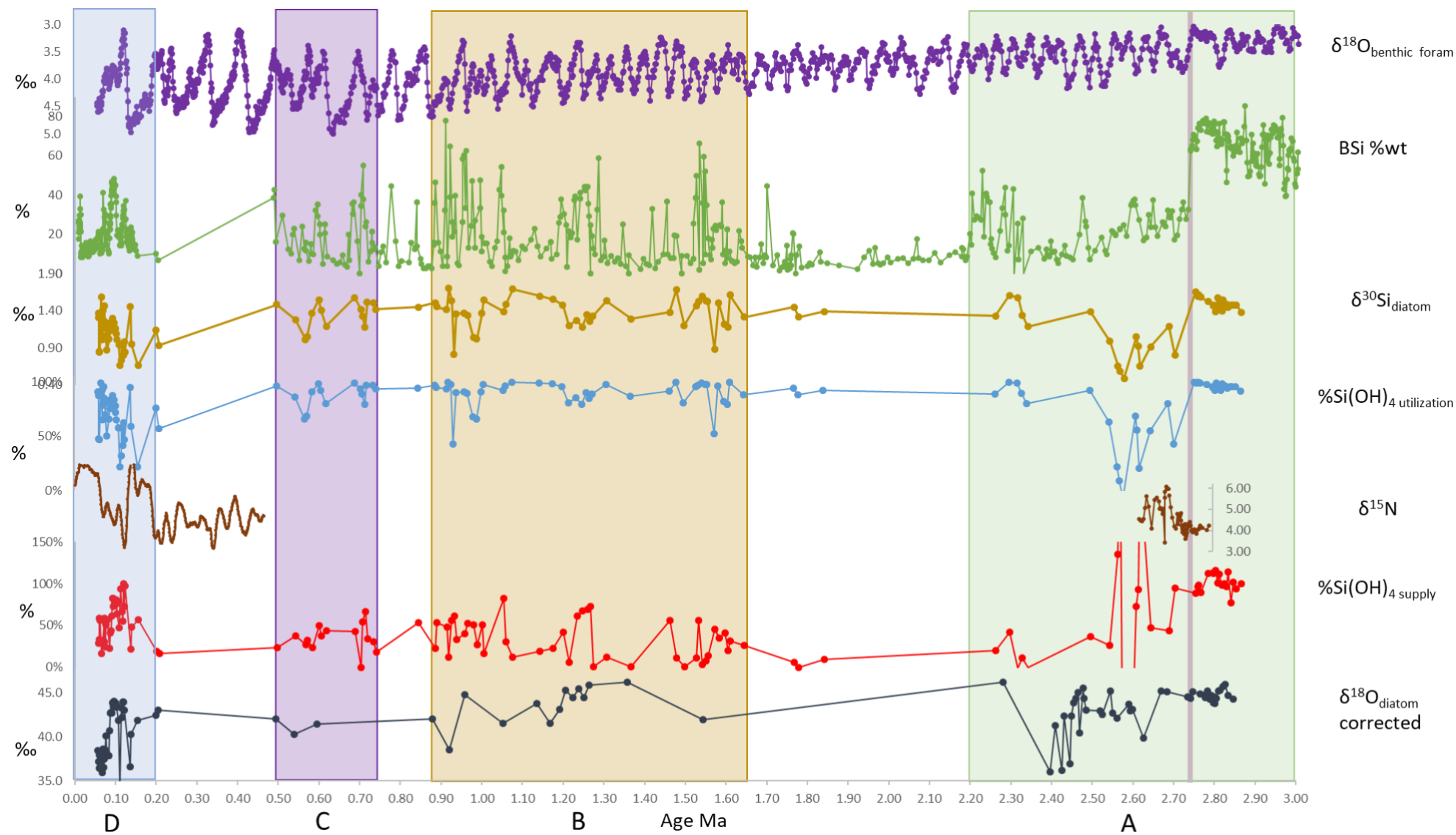


734

735 Figure 3: Scanning electron microscope (SEM) images of clean diatom samples from ODP Site 882.

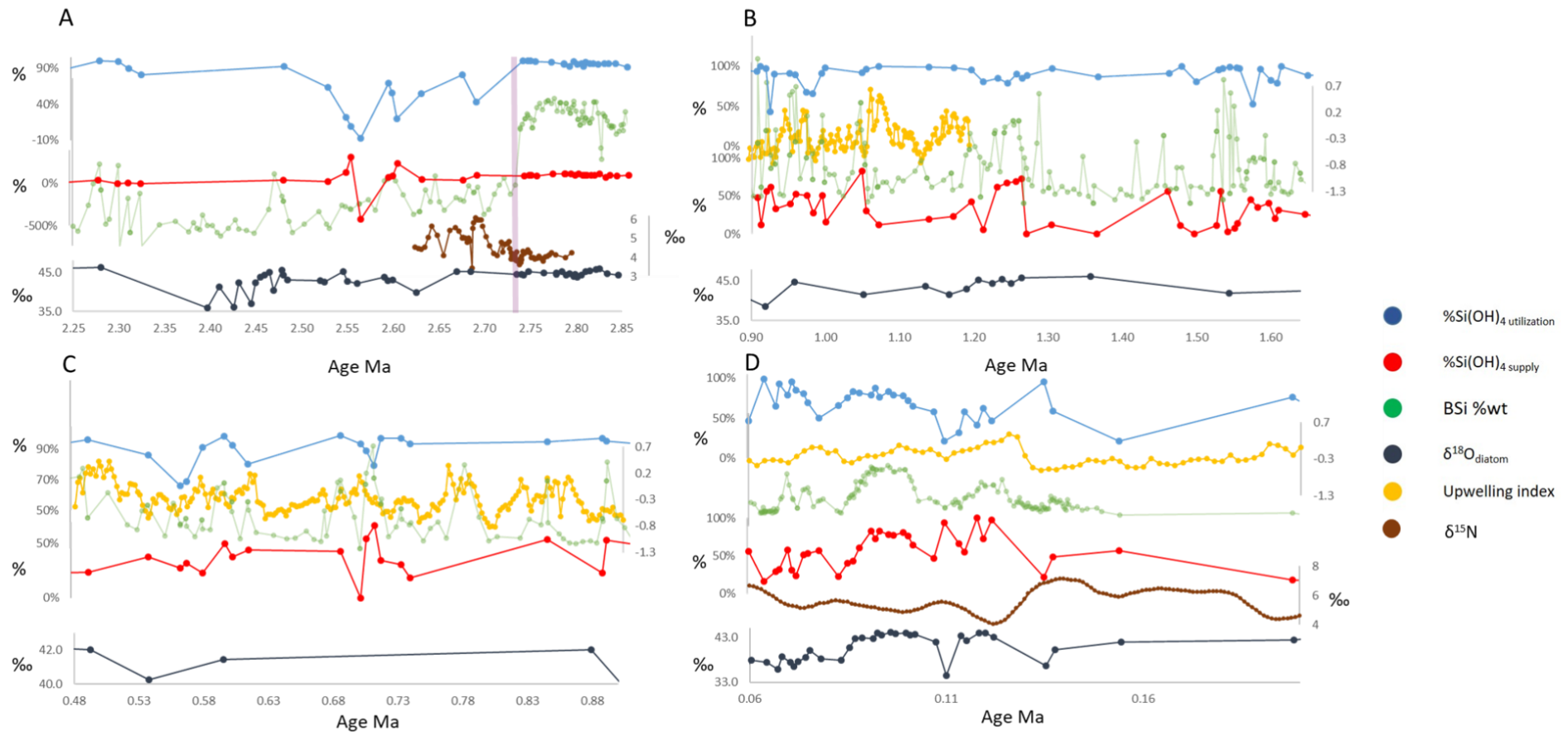
736

737



738

739 Figure 4 [colour]: Data from ODP Site 882 showing changes in the LR04 benthic foraminifera  $\delta^{18}\text{O}$  record ( $\delta^{18}\text{O}_{\text{benthic foram.}}$ )  
 740 (Lisecki and Raymo 2004), opal concentration (BSi %wt) (Swann 2010, Bailey et al., 2011, Swann and Snelling 2015),  $\delta^{30}\text{Si}_{\text{diatom}}$ , nutrient consumption  
 741 ( $\% \text{Si(OH)}_4$  utilisation),  $\delta^{15}\text{N}_{\text{bulk}}$  (0-0.5 Ma Galbraith et al., 2008; 2.6-2.8 Ma Studer et al., (2012; pers comm.)) nutrient supply ( $\% \text{Si(OH)}_4$  supply) and fresh  
 742 water input ( $\delta^{18}\text{O}_{\text{diatom}}$  corrected). Shaded areas relate to sections discussed in the text. Purple line at 2.73 Ma marks NHG.



744

745 Figure 5A-D [colour]: Detailed Data from ODP Site 882 showing changes in the opal concentration (BSi %wt), nutrient consumption (%Si(OH)<sub>4</sub> utilisation),  
746 nutrient supply (%Si(OH)<sub>4</sub> supply) and fresh water input ( $\delta^{18}\text{O}_{\text{diatom}}$  corrected). The Bering Sea upwelling index (Worne et al 2019) is shown where data is  
747 available as is  $\delta^{15}\text{N}$  from Studer et al., (2.8-2.6 Ma) (2012., pers comm.) and Galbraith 2008 (0.06-2 Ma) (BSi %wt is shown in the background in  
748 green). Purple line at 2.73 Ma marks NHG.

749